LETTER

https://doi.org/10.1038/s41586-019-0952-6

Verified quantum information scrambling

K. A. Landsman[1]*, C. Figgatt[1,6], T. Schuster[2], N. M. Linke[1], B. Yoshida[3], N. Y. Yao[2,4] & C. Monroe[1,5]

Quantum scrambling is the dispersal of local information into many-body quantum entanglements and correlations distributed throughout an entire system. This concept accompanies the dynamics of thermalization in closed quantum systems, and has recently emerged as a powerful tool for characterizing chaos in black holes[1–4]. However, the direct experimental measurement of quantum scrambling is difficult, owing to the exponential complexity of ergodic many-body entangled states. One way to characterize quantum scrambling is to measure an out-of-time-ordered correlation function (OTOC); however, because scrambling leads to their decay, OTOCs do not generally discriminate between quantum scrambling and ordinary decoherence. Here we implement a quantum circuit that provides a positive test for the scrambling features of a given unitary process[5,6]. This approach conditionally teleports a quantum state through the circuit, providing an unambiguous test for whether scrambling has occurred, while simultaneously measuring an OTOC. We engineer quantum scrambling processes through a tunable three-qubit unitary operation as part of a seven-qubit circuit on an ion trap quantum computer. Measured teleportation fidelities are typically about 80 per cent, and enable us to experimentally bound the scrambling-induced decay of the corresponding OTOC measurement.

The dynamics of strongly interacting quantum systems lead to the local memory loss of initial conditions, analogous to the chaotic behaviour of classical systems. At first glance, this appears inconsistent with the reversible or unitary nature of quantum time-evolution. The resolution lies in the fact that such local quantum information generically becomes delocalized throughout the entire system, and thus hidden in nonlocal degrees of freedom. This quantum scrambling process has sharpened our understanding of the limits of thermalization and chaos in quantum systems[1–4]. At one extreme, certain disordered systems can evade thermalization entirely, leading to the slow logarithmic spread of quantum information[7]. At the other extreme, the existence of a maximum speed limit for thermalization—known as 'fast-scrambling'—is conjectured to occur in certain large-N gauge theories[8] as well as the dynamics of black holes[1–4]. Synergy with the latter extends both ways: many of the tools and ideas originally developed in the context of black hole physics[9–12] have been found to be useful in characterizing the scrambling behaviour of generic many-body systems.

These wide-ranging impacts of quantum scrambling have stimulated the search for experimental evidence[13–19] of scrambling dynamics that could help shed light on quantum non-equilibrium processes in exotic materials[20,21] and the fast-scrambling dynamics of black holes[1–4]. Recent work has focused on so-called OTOCs[3,4,22], which take the form $\langle \hat{V}^\dagger \hat{W}^\dagger(t) \hat{V} \hat{W}(t) \rangle$, where $\hat{V}$ and $\hat{W}$ are unitary operators acting on separate subsystems. The operator $\hat{W}(t) = \hat{U}^\dagger \hat{W} \hat{U}$ is the time-evolved version of W under the unitary operator $\hat{U} = e^{-i\mathcal{H}t}$ generated through either a Hamiltonian $\mathcal{H}$ or an equivalent digital quantum circuit. As scrambling proceeds, $\hat{W}(t)$ becomes increasingly nonlocal, causing the OTOC to decay[23], which is taken as an experimental indication of scrambling[15–18].

However, it is difficult to distinguish between information scrambling and extrinsic decoherence in the OTOC's temporal decay. For example, non-unitary time-evolution arising from depolarization or classical noise processes naturally lead the OTOC to decay, even in the absence of quantum scrambling. A similar decay can also originate from even slight mismatches between the purported forward and backwards time-evolution of $\hat{W}(t)$ (refs [6,16] and [24]). Although full quantum tomography can in principle distinguish scrambling from decoherence and experimental noise, this requires a number of measurements that scales exponentially with system size and is thus impractical.

In this work, we overcome this challenge and implement a quantum teleporation protocol that robustly distinguishes information scrambling from both decoherence and experimental noise[5,6]. Using this protocol, we demonstrate verifiable information scrambling in a family of unitary circuits and provide a quantitative bound on the amount of scrambling observed in the experiments.

The intuition behind our approach lies in a re-interpretation of the black-hole information paradox[9,10], under the assumption that the dynamics of the black hole can be modelled as a random unitary operation $\hat{U}$ (Fig. 1). Schematically, an observer (Alice) throws a secret quantum state into a black hole, while an outside observer (Bob) attempts to reconstruct this state by collecting the Hawking radiation emitted at a later time[1,10].

An explicit decoding protocol has been recently proposed[5,6], which enables Bob to decode Alice's state using a quantum memory, an ancillary entangled pair of qubits, and knowledge of the effective black-hole unitary $\hat{U}$ (ref. [25]). The protocol requires Bob to apply $\hat{U}^*$ to his own quantum memory and one half of the ancillary entangled pair. Following this, Bob performs a projective measurement, which plays the part of teleporting Alice's secret quantum state to the reference qubit in Bob's ancillary entangled pair. The successful decoding of Alice's quantum information is only possible because of the maximally scrambling dynamics of the unitary, which ensure that the information about Alice's secret state is almost immediately distributed throughout the entire system[1,26]. Since maximally scrambling dynamics are requisite for successful teleportation, the teleportation fidelity provides a fail-safe diagnostic for true quantum information scrambling (see Methods section 'Brief overview of quantum teleportation').

Unlike a direct measurement of OTOCs, this protocol can explicitly distinguish scrambling from either decoherence or a mismatch between forward and backward time-evolution (that is, the encoding and decoding unitaries $\hat{U}$ and $\hat{U}^*$). Moreover, the success probability of the projective measurement provides an independent measure of the average experimental value of the OTOC, which includes the effects of both noise and decoherence[6]. By comparing the teleportation fidelity and the success probability, one can quantitatively and unambiguously bound the amount of quantum scrambling by the unitary operation $\hat{U}$.

We experimentally implement the above teleportation protocol on a seven-qubit fully connected quantum computer[27] using a family of three-qubit scrambling unitaries $\hat{U}_s$. Our quantum computer is realized with a crystal of trapped atomic $^{171}Yb^+$ ion qubits, defined by the hyperfine 'clock' states, as described in Methods section 'Experimental details'. We confine nine ions in the linear ion trap and use the nearly equally spaced middle seven ions for the circuit. We can drive single qubit gates on any of the seven qubits with a typical fidelity of 99.0(5)%

[1]Joint Quantum Institute, Department of Physics and Joint Center for Quantum Information and Computer Science, University of Maryland, College Park, MD, USA. [2]Department of Physics, University of California Berkeley, Berkeley, CA, USA. [3]Perimeter Institute for Theoretical Physics, Waterloo, Ontario, Canada. [4]Materials Science Division, Lawrence Berkeley National Laboratory, Berkeley, CA, USA. [5]IonQ Inc., College Park, MD, USA. [6]Present address: Honeywell., Broomfield, CO, USA. *e-mail: kalands@umd.edu

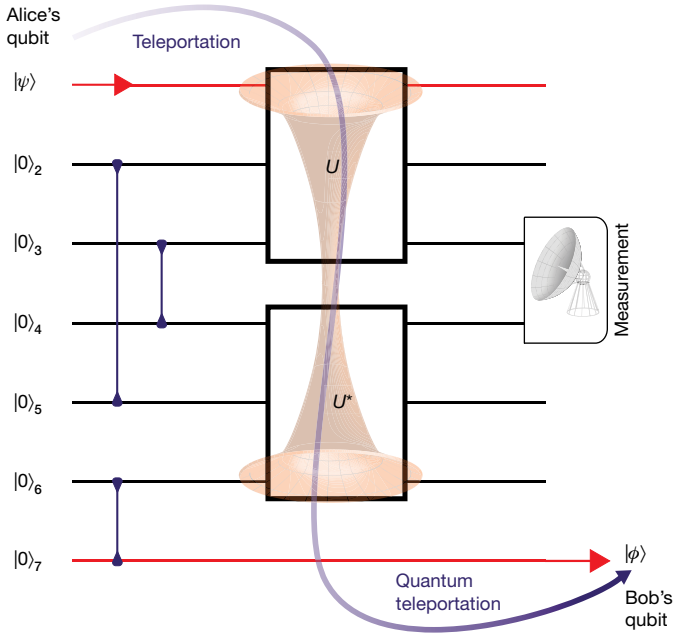

Fig. 1 | Experimental quantum circuit. Schematic of our 7-qubit circuit, which uses quantum teleportation to detect information scrambling. Qubit 1 represents the state to be teleported, while the remaining six qubits are prepared in EPR pairs (vertical lines). The first three qubits are acted on by the unitary, $\hat{U}$, whose scrambling properties are to be characterized. To perform teleportation, qubits 4 to 6 are acted on by the conjugate unitary $\hat{U}^*$, and a projective EPR measurement is performed on any pair of qubits: (3, 4), (2, 5) or (1, 6). If the unitary $\hat{U}$ is maximally scrambling, the information stored in qubit 1 is delocalized, and decoding becomes possible, as seen by the measurement-heralded teleportation of qubit 1's state to qubit 7. The underlay depicts an analogy between our protocol and information propagation through a traversable wormhole[11,12]; within this interpretation, Alice attempts to teleport her qubit to Bob, who has control over qubits 3 to 7. This interpretation is further clarified in the discussions.

and entangling two-qubit gates on any pair of qubits with a typical fidelity of 98.5(5)% (see Methods section 'Experimental details'). Projective measurements of the qubits in any basis are performed with standard fluorescence techniques[28], with a qubit readout fidelity of 99.4(1)%. In combination, Bell state preparation and measurement can be performed with a fidelity of 98(1)% and are generated by a compiler that pieces together native, one- and two-qubit gates to produce the desired gates in a modular fashion[27].

A schematic of the experiment is depicted in Fig. 1. The first qubit is prepared in a designated single-qubit state $|\psi\rangle$. We initialize the six additional qubits in three Einstein–Podolsky–Rosen (EPR) pairs, $|\mathrm{EPR}\rangle = \frac{1}{\sqrt{2}}(|00\rangle + |11\rangle)$, between qubits (2, 5), (3, 4) and (6, 7). We perform the scrambling unitary $\hat{U}_s$ on qubits 1 to 3, and the decoding unitary $\hat{U}_d = \hat{U}_s^*$ on qubits 4 to 6. The explicit form of these unitaries and their decompositions into two-qubit gates is detailed in Methods section 'Implementing and optimizing scrambling operators'. We complete the decoding protocol by projectively measuring any designated pair of qubits—a chosen qubit $p \in \{1, 2, 3\}$ and its complement qubit $(7-p) \in \{4, 5, 6\}$—onto an EPR pair. In the absence of decoherence and errors, the probability P_ψ of a successful projective measurement can be directly related to the OTOC by:

$$P_\psi = \sum_{\phi,\hat{O}_P} \langle \hat{O}_1^\dagger \hat{O}_P^\dagger(t) \hat{O}_1 \hat{O}_P(t) \rangle \qquad (1)$$

where $\hat{O}_1 \equiv |\psi\rangle\langle\phi|$ acts on qubit 1, $\sum_{\phi,\hat{O}_P}$ denotes an average over single-qubit quantum states ϕ and the Pauli operators $\hat{O}_P$ acting on the projectively measured qubit, and[5,6] $\hat{O}_P(t) = \hat{U}_s^\dagger \hat{O}_P \hat{U}_s$. If the EPR projection is successful, the decoding of the initial state $|\psi\rangle$ can be quantified via the teleportation fidelity: $F_\psi = |\langle\varphi|\psi\rangle|^2$, where $|\varphi\rangle$ is the final state of the ancillary qubit 7. To characterize the nature of different scrambling unitaries, we repeat this protocol for initial states $|\psi\rangle \in \{|0_x\rangle, |1_x\rangle, |0_y\rangle, |1_y\rangle, |0_z\rangle, |1_z\rangle\}$, where $|0(1)_\alpha\rangle$ denotes the positive (negative) eigenstate of the Pauli operator σ_α.

We begin by illustrating the challenge associated with interpreting conventional OTOC experimental measurements[15–18]. In particular, we perform a control experiment with a non-scrambling unitary in the presence of deliberate experimental errors (Fig. 2a): specifically, we take $\hat{U}_s$ to be the identity operation, and introduce single-qubit rotational errors (parameterized by strength θ) following the operation of $\hat{U}_s$, but not the decoding operation $\hat{U}_d$, creating a mismatch between forward and backward time-evolution. To allow for a fair comparison with the case of maximally scrambling unitaries, we implement the identity operator as a combination of one- and two-qubit gates of comparable complexity (and total number). As we increase the size of the mismatch error, we see that the average OTOC (as measured by P_ψ) decays, consistent with the expected sensitivity of the OTOC to experimental noise (Fig. 2). Crucially however, the decoding fidelity remains constant near 50%, the expected fidelity for an unknown qubit state, confirming that no scrambling has taken place.

In the ideal case, both the teleportation fidelity (F_ψ) and the average OTOC (P_ψ) probe only scrambling and are thus redundant. This is reflected in the error-free relation $d_1[(d_1+1)\langle F_\psi P_\psi\rangle - \langle P_\psi\rangle] = 1$, where d_1 is the dimension of the initial state $|\psi\rangle$ (in our case, $d_1 = 2$) and the average is performed over all initial states. Decoherence and experimental error lead to deviations from this relation, which we quantify with the effective noise factor[6]

$$\mathcal{N} \equiv d_1[(d_1+1)\langle F_\psi P_\psi\rangle - \langle P_\psi\rangle] \qquad (2)$$

whose decay from unity signals the presence of error-induced OTOC decay in our quantum circuit. Note that $\mathcal{N} = 1$ in the ideal case and $\mathcal{N} = 0.25$ (that is, $1/d_1^2$) in the fully decohered case. As expected, the observed $\mathcal{N}$ decreases with increasing mismatch (Fig. 2e), reflecting the deliberate error-induced decay of the OTOC, despite the lack of any quantum scrambling dynamics. Moreover, the measured value of $\mathcal{N} \approx 0.60$–0.75 at zero mismatch ($\theta = 0$) reflects the inherent errors in the experiment, which are expected from the many gates comprising the EPR preparation, unitary operation and EPR measurement.

With the control experiment in hand, we now characterize information scrambling for a family of unitary operators $\hat{U}_s(\alpha)$ that continuously interpolate (Fig. 2b) between the identity operator ($\alpha = 0$) and a maximally scrambling unitary ($\alpha = 1$), as described in Methods section 'Implementing and optimizing scrambling operators'. The gate decomposition of the $\hat{U}_s(\alpha)$ operation varies only in single-qubit rotations about the z-axis, which are performed classically with negligible error. Similar to the previous case, we observe the average OTOC to decay as the scrambling parameter, α, is tuned from 0 to 1, as shown in Fig. 2c. However, unlike the case of the deliberate mismatch-error in Fig. 2a, the OTOC decay is accompanied by an increase in the decoding teleportation fidelity, indicating the presence of true quantum information scrambling. Measurement of a relatively constant noise factor confirms that the experimental error does not depend strongly on the parameter α and thus cannot fully account for the decay of the OTOC. In our system, the error scales with the number and type of gates, which are constant across the interpolation.

Using our experimentally measured noise factor $\mathcal{N}$, we can bound the true, scrambling-induced decay of the OTOC for error-free time-evolution via the unitaries $\hat{U}_s(\alpha)$. Assuming that extrinsic decoherence is negligible (that is, that coherent errors dominate the experiment), we find that the ideal average OTOC can be upper-bounded by[6]: $4\langle P_\psi\rangle^2/\mathcal{N}^2$. Therefore, we can experimentally upper-bound the value of the OTOC for the maximally scrambling unitary, $\hat{U}_s(\alpha = 1)$, by approximately 0.47(2).

To demonstrate that our scrambling unitaries are indeed delocalizing information across the entire system, we show that teleportation succeeds independently of the chosen subsystem partition. To do this,

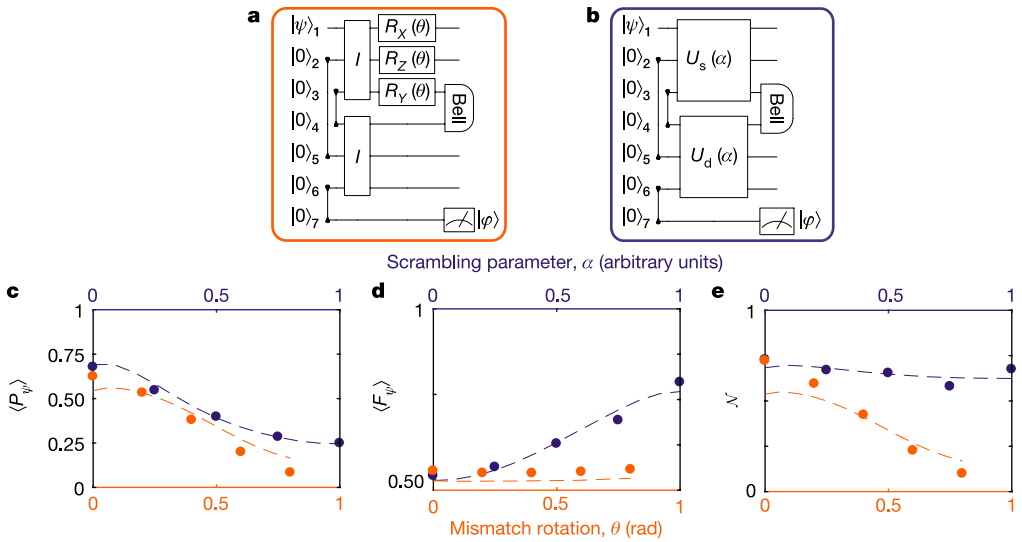

Fig. 2 | Quantum scrambling parameterization. a, Circuit designed to demonstrate that a mismatch between $\hat{U}_s$ and $\hat{U}_d$ naturally leads to the decay of the OTOC without enabling teleportation. Following the $\hat{U}_s = I$ operation, we perform three additional independent rotations R_X, R_Y and R_Z on the qubits by angle θ and measure the state of qubit 7, $|\varphi\rangle$. Accompanying data (orange symbols) for the averaged successful projective measurement $\langle P_\psi \rangle$, averaged teleportation fidelity $\langle F_\psi \rangle$ and noise factor $\mathcal{N}$ as a function of θ are depicted in **c**, **d** and **e**. **b**, Circuit designed to probe the OTOC and teleportation fidelity as a function of the scrambling parameter α with $\alpha = 0$ representing no scrambling and $\alpha = 1$ representing full scrambling. Accompanying data (purple symbols) for $\langle P_\psi \rangle$, $\langle F_\psi \rangle$ and $\mathcal{N}$ as a function of θ are depicted in **c**, **d** and **e**. **c**–**e**, For the mismatch circuit shown in **a**, we find that the teleportation fidelity remains near its minimal value, $\langle F_\psi \rangle \approx 0.5$, for all θ, consistent with our expectation that scrambling is not occurring. However, one observes that the OTOC (as measured via $\langle P_\psi \rangle$) decays to nearly zero, which would nominally suggest scrambling. This is precisely the challenge with interpreting OTOC measurements as an indicator of scrambling in noisy experiments. Finally, as expected, we observe that the noise parameter $\mathcal{N}$ decays as the mismatch grows. For the tunable scrambling circuit shown in **b**, we find that the teleportation fidelity increases as we increase our scrambling parameter α. This increase in teleportation fidelity is accompanied by a decrease in the OTOC (as measured via $\langle P_\psi \rangle$), indicating that the OTOC's decay is caused, at least in part, by true scrambling dynamics. Finally, the noise parameter $\mathcal{N}$ remains relatively constant because the complexity and therefore experimental errors associated with implementing $\hat{U}(\alpha)$ are mostly α-independent. Dashed lines represent theory curves that are obtained via numerical simulations of the circuit assuming a one-parameter coherent error model (see Methods for details). Error bars indicating statistical uncertainties are smaller than the data points and are omitted. Deviations between simulations and data are probably caused by systematic errors, such as experimental drift and imperfect calibration. Data represented are obtained by averaging 18,000 experimental repitions, 3,000 for each of the six teleported states described in the main text.

we select three different pairs of qubits to be projectively measured in the final decoding step, corresponding to the three qubits acted upon by the scrambling unitary $\hat{U}_s$. Decoding succeeds with a fidelity of 70–80% for all projectively measured pairs and all initial states (Fig. 3). By contrast, the same protocol applied to the non-scrambling identity operator results in a nontrivial decoding fidelity for only a single pair, in which case the entire protocol reduces to the standard setup for quantum teleportation (Fig. 3). Taken together, these measurements demonstrate the full delocalization of the initially local information of the input state $|\psi\rangle$ via the maximally scrambling unitary $\hat{U}_s$.

Intriguingly, time-evolution that is not maximally scrambling may nevertheless scramble some subset of information. For example, in strongly disordered systems, localization can lead to the scrambling of phase information but not the scrambling of population[7]; this situation would correspond to a sort of 'classical scrambler' wherein teleportation only occurs for z-basis states. Such classical scramblers may provide insight into connections between quantum and

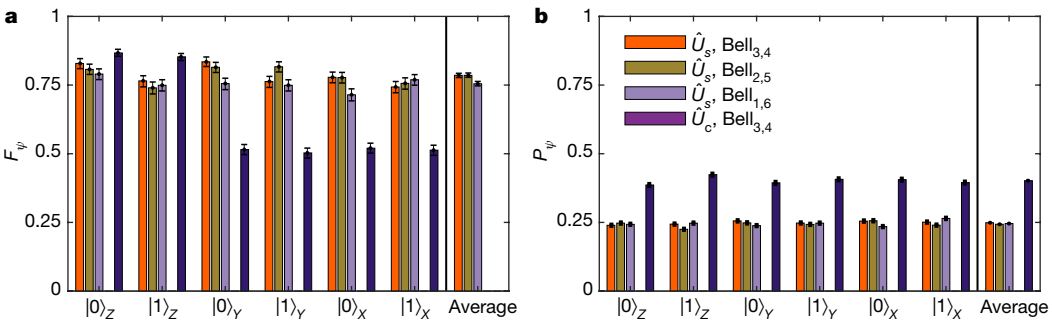

Fig. 3 | Teleportation of Pauli operator eigenstates. a, Teleportation fidelities F_ψ for maximally scrambling ($\hat{U}_s(\alpha = 1)$) and classically scrambling ($\hat{U}_c$) unitaries are presented for all teleported states as well as all subsystems {3, 4}, {2, 5} and {1, 6} that were used for the projective measurement (indicated as different bar colours). In the case of the maximally scrambling unitary, all basis states and all measurement Bell pairs lead to successful teleportation, demonstrating the full delocalization of Alice's quantum state. In the case of the classical scrambling unitary, we projectively measure on subsystem {3, 4}. Only the z-basis states are successfully teleported. Data (for $\hat{U}_s$) averaged over all six teleported states is shown in the final column. Data are depicted with the same colour scheme as in **b**. **b**, Measurements of P_ψ from the experiments described in **a**. The probabilities averaged over all basis states constitutes the average experimental OTOC. Error bars indicate statistical uncertainties. Experimental data points are calculated by averaging over 4,000 data points.

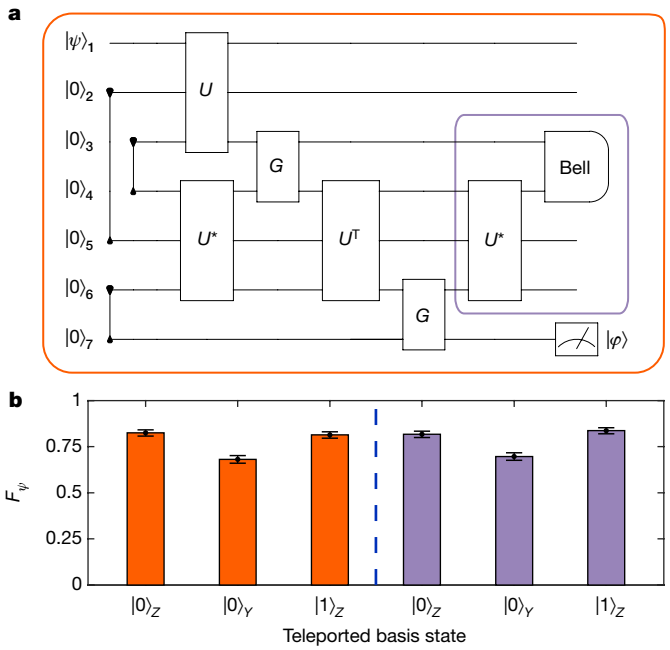

Fig. 4 | Deterministic teleportation with a Grover variant. a, Circuit diagram for our deterministic teleportation scheme that utilizes a built-in Grover's search protocol. Ideally, this search finds the desired EPR state with perfect fidelity. By adding in post-selection (purple outline), we can quantify the performance of the search. **b**, Depicts the measured teleportation fidelity for different initial states using the Grover search protocol, both with and without post-selection. The average fidelity without post-selection (orange) is 77(2)% and with post-selection (purple) is 78(2)%.

classical chaos; moreover, measurements of state- and unitary-dependent scrambling may help to diagnose errors more precisely in digital many-body quantum simulations[29,30].

Thus far, our decoding protocols have all been probabilistic: they rely upon an EPR projective measurement to teleport the unknown quantum state. While the success probability of this EPR projection enables us to quantify the error-induced decay of the OTOC, one can also implement a deterministic version of the decoding protocol[5,6] (Fig. 4a). The intuition behind this deterministic decoder is to perform a search for the EPR pair through an implementation of Grover's algorithm[31] instead of post-selecting on a projective measurement (see in Methods section 'Brief overview of Grover's algorithm'). Scrambling remains the focus of this version; while the deterministic decoding fidelity can be lower-bounded by four-point OTOCs (similar to those in equation (1)), their precise measurement actually corresponds to certain averages of higher-point OTOCs. Such higher-point OTOCs[3] can serve as more fine-grained measures of chaos beyond four-point OTOCs, and may be able to diagnose higher moments of quantum randomness. Within the Grover-search variant of our decoding protocol, three states are deterministically decoded with an average fidelity of 77(2)% (Fig. 4b).

Finally, we perform a further variation of this protocol that reintroduces a projective measurement as a means of purifying errors from the experiment, while retaining the same decoding strategy as above. Here, the same three initial states were decoded with an average fidelity of 78(2)% (Fig. 4b). That this purification leads to the same teleportation fidelity despite the additional gate depth (Fig. 4a, purple box) suggests that the fidelity of the EPR Grover search is roughly 85%. To demonstrate the generality of our approach, these Grover-based protocols were performed with a different class of maximally scrambling unitaries from the previous probabilistic protocol, as described in Methods section 'Implementing and optimizing scrambling operators'.

Thus far, we have alluded to connections between our teleportation protocol and the scrambling dynamics of black holes. By further elucidating this analogy, we hope to motivate future experiments as well as clarify our own. Interestingly, the scrambling-induced teleportation observed in our experiment can be reinterpreted as simulating the propagation of information through a traversable wormhole that connects a pair of black holes (depicted schematically in Fig. 1)[25,32]. This reinterpretation is based upon the so-called Hayden–Preskill thought experiment, which demonstrates that one can utilize a quantum memory entangled with the black hole to decode information scrambled by the black hole[1,10]. In our experiment, qubit 1 contains the information to be scrambled and subsequently decoded. The EPR pairs (2, 5) and (3, 4) are analogous to the black hole entangled with a quantum memory, while (6, 7) is an ancillary EPR pair necessary to perform the decoding.

Our work opens the door to a number of intriguing future directions. First, by experimentally scaling to larger circuits, one should be able to probe the scrambling dynamics of Haar random unitaries, complementary to the scramblers studied here. Since the teleportation protocol enables the built-in verification of scrambling, it may provide a natural method for directly measuring the randomness intrinsic to such circuits. Second, while we have focused on the challenges of distinguishing between scrambling and decoherence in this work, our protocol suggests that scrambling circuits may provide a near-term method to benchmark and verify large-scale quantum simulations[30]. In particular, by probing the teleportation fidelity as a function of both input state complexity and circuit, many-body noise mechanisms could be measured that would be invisible to typical single- and two-qubit randomized benchmarking methods[33]. Finally, although our unitary is implemented as a digital quantum circuit, one could also choose to implement a unitary via Hamiltonian time evolution and to track the scrambling behaviour as a function of time.

Online content

Any methods, additional references, Nature Research reporting summaries, source data, statements of data availability and associated accession codes are available at https://doi.org/10.1038/s41586-019-0952-6.

Received: 7 June 2018; Accepted: 8 January 2019;
Published online 6 March 2019.

1. Hayden, P. & Preskill, J. Black holes as mirrors: quantum information in random subsystems. *J. High Energy Phys.* **2007**, 120 (2007).
2. Kitaev, A. A simple model of quantum holography. http://online.kitp.ucsb.edu/online/entangled15/kitaev/ (2015).
3. Shenker, S. H. & Stanford, D. Black holes and the butterfly effect. *J. High Energy Phys.* **2014**, 67 (2014).
4. Maldacena, J., Shenker, S. H. & Stanford, D. A bound on chaos. *J. High Energy Phys.* **2016**, 106 (2016).
5. Yoshida, B. & Kitaev, A. Efficient decoding for the Hayden-Preskill protocol. Preprint at http://arxiv.org/abs/1710.03363 (2017).
6. Yoshida, B. & Yao, N. Y. Disentangling scrambling and decoherence via quantum teleportation. *Phys. Rev. X* **9**, 011006 (2018).
7. Nandkishore, R. & Huse, D. A. Many-body localization and thermalization in quantum statistical mechanics. *Ann. Rev. Condensed Matter Phys.* **6**, 15–38 (2015).
8. Maldacena, J. The large-*N* limit of superconformal field theories and supergravity. *Int. J. Theor. Phys.* **38**, 1113 (1999).
9. Hawking, S. W. Breakdown of predictability in gravitational collapse. *Phys. Rev. D* **14**, 2460–2473 (1976).
10. Page, D. N. Average entropy of a subsystem. *Phys. Rev. Lett.* **71**, 1291–1294 (1993).
11. Gao, P., Jafferis, D. L. & Wall, A. C. Traversable wormholes via a double trace deformation. *J. High Energy Phys.* **2017**, 151 (2017).
12. Maldacena, J., Stanford, D. & Yang, Z. Diving into traversable wormholes. *Fortschr. Phys.* **65**, 1700034 (2017).
13. Swingle, B., Bentsen, G., Schleier-Smith, M. & Hayden, P. Measuring the scrambling of quantum information. *Phys. Rev. A* **94**, 040302 (2016).
14. Yao, N. Y. et al. Interferometric approach to probing fast scrambling. Preprint at http://arxiv.org/abs/1607.01801 (2016).
15. Li, J. et al. Measuring out-of-time-order correlators on a nuclear magnetic resonance quantum simulator. *Phys. Rev. X* **7**, 031011 (2017).
16. Gärttner, M. et al. Measuring out-of-time-order correlations and multiple quantum spectra in a trapped-ion quantum magnet. *Nature Phys.* **13**, 781–786 (2017).

17. Meier, E. J., Ang'ong'a, J., An, F. A. & Gadway, B. Exploring quantum signatures of chaos on a Floquet synthetic lattice. Preprint at http://arxiv.org/abs/1705.06714 (2017).
18. Wei, K. X., Ramanathan, C. & Cappellaro, P. Exploring localization in nuclear spin chains. *Phys. Rev. Lett.* **120**, 070501 (2018).
19. Yunger Halpern, N., Swingle, B. & Dressel, J. Quasiprobability behind the out-of-time-ordered correlator. *Phys. Rev. A* **97**, 042105 (2018).
20. Blake, M., Davison, R. A. & Sachdev, S. Thermal diffusivity and chaos in metals without quasiparticles. *Phys. Rev. D* **96**, 106008 (2017).
21. Banerjee, S. & Altman, E. Solvable model for a dynamical quantum phase transition from fast to slow scrambling. *Phys. Rev. B* **95**, 134302 (2017).
22. Larkin, A. I. & Ovchinnikov, Y. N. Quasiclassical method in the theory of superconductivity. *Sov. Phys. JETP* **28**, 1200–1205 (1969).
23. Roberts, D. A., Stanford, D. & Susskind, L. Localized shocks. *J. High Energy Phys.* **2015**, 51 (2015).
24. Swingle, B. & Yunger Halpern, N. Resilience of scrambling measurements. *Phys. Rev. A* **97**, 062113 (2018).
25. Maldacena, J. & Susskind, L. Cool horizons for entangled black holes. *Fortschr. Phys.* **61**, 781–811 (2013).
26. Hosur, P., Qi, X.-L., Roberts, D. A. & Yoshida, B. Chaos in quantum channels. *J. High Energy Phys.* **2016**, 4 (2016).
27. Debnath, S. et al. Demonstration of a small programmable quantum computer with atomic qubits. *Nature* **536**, 63–66 (2016).
28. Olmschenk, S. et al. Manipulation and detection of a trapped Yb^+ hyperfine qubit. *Phys. Rev. A* **76**, 052314 (2007).
29. Lanyon, B. P. et al. Universal digital quantum simulation with trapped ions. *Science* **334**, 57–61 (2011).
30. Cirac, J. I. & Zoller, P. Goals and opportunities in quantum simulation. *Nat. Phys.* **8**, 264–266 (2012).
31. Grover, L. K. in *Proc. Twenty-eighth Annual ACM Symposium on Theory of Computing* (STOC '96) 212–219 (ACM, New York, 1996); https://doi.org/10.1145/237814.237866.
32. Maldacena, J. Eternal black holes in anti-de Sitter. *J. High Energy Phys.* **2003**, 021 (2003).
33. Knill, E. et al. Randomized benchmarking of quantum gates. *Phys. Rev. A* **77**, 012307 (2008).

Acknowledgements We gratefully acknowledge discussions with R. Bousso, D. Harlow, F. Machado, I. Siddiqi, L. Susskind and Q. Zhuang. Additionally, we thank E. Edwards for the development of Fig. 1. This work is supported in part by the ARO through the IARPA LogiQ programme, the AFOSR MURI on Quantum Measurement and Verification, the ARO MURI on Modular Quantum Circuits, the DOE ASCR Program, and the NSF Physics Frontier Center at JQI. T.S. and N.Y.Y. acknowledge support from the Office of Science, Office of High Energy Physics of the US Department of Energy under contract number DE-AC02-05CH11231 through the COMPHEP pilot "Probing information scrambling via quantum teleportation" and the Office of Advanced Scientific Computing Research, Quantum Algorithm Teams Program. Research at the Perimeter Institute is supported by the Government of Canada through Innovation, Science and Economic Development Canada and by the province of Ontario through the Ministry of Economic Development, Job Creation and Trade. T.S. acknowledges support from the National Science Foundation Graduate Research Fellowship Program under grant number DGE 1752814.

Reviewer information *Nature* thanks Daniel Harlow and the other anonymous reviewer(s) for their contribution to the peer review of this work.

Author contributions K.A.L., C.F., N.M.L. and C.M. all contributed equally to the data collection and analysis presented in this manuscript. T.S. and N.Y.Y. contributed equally to the numerical simulation. All authors contributed equally in designing and planning experiments.

Competing interests The authors declare competing interests: C.M. is a founding scientist of IonQ, Inc.

Additional information
Extended data is available for this paper at https://doi.org/10.1038/s41586-019-0952-6.
Reprints and permissions information is available at http://www.nature.com/reprints.
Correspondence and requests for materials should be addressed to K.A.L.
Publisher's note: Springer Nature remains neutral with regard to jurisdictional claims in published maps and institutional affiliations.

METHODS

Experimental details. *Trapped ion qubits.* We perform the experiment on a quantum computer consisting of a chain of nine $^{171}Yb^{+}$ ions confined in a Paul trap and laser-cooled near the motional ground state. The hyperfine-split $^{2}S_{1/2}$ ground level with an energy difference of 12.642821 GHz provides a pair of qubit states, $|0\rangle = |0, 0\rangle$ and $|1\rangle = |1, 0\rangle$ with quantum numbers $|F, m_F\rangle$, that are magnetic field independent to first order. The 1/e-coherence time of this so-called 'atomic clock' qubit is 1.5(5) s in our system, limited by magnetic field noise. Optical pumping is used to initialize the state of all ions, and the final states are measured collectively via state-dependent fluorescence detection[28]. Each ion is mapped to a distinct channel of a photomultiplier tube array. The average state detection fidelity is 99.4(1)% for a single qubit, while a 7-qubit state is typically read out with 92(1)% average fidelity, limited by channel-to-channel crosstalk. These state detection and measurement (SPAM) errors are characterized in detail by measuring the state-to-state error matrix.

Gate operations. Quantum operations are achieved by applying two Raman beams from a single 355-nm mode-locked laser, which form beat notes near the qubit frequency. The first Raman beam is a global beam applied to the entire chain, while the second is split into individual addressing beams to target each ion qubit (see Extended Data Fig. 1)[27], controlled by a set of arbitrary waveform generators. Single-qubit gates are generated by driving resonant Rabi rotations (R-gates) of defined phase, amplitude and duration. Single-qubit Z-rotations are applied efficiently as classical phase advances. Two-qubit gates (XX-gates) are realized by illuminating two ions with beat-note frequencies near the motional sidebands and creating an effective spin–spin Ising interaction via transient entanglement between the state of two ions and all modes of motion[34]. To ensure that the motion is left disentangled from the qubit states at the end of the interaction, we employ a pulse shaping scheme[35,36]. We use only the middle seven ions in the chain as qubits, in order to ensure a higher uniformity in the ion spacing, matching the equally spaced individual addressing beams. The two edge ion qubits are neither manipulated nor measured, but their contribution to the collective motion is included when creating the entangling operations.

Bell state preparation and measurement. In Fig. 2b, we depict Bell state pairs initially in the state $\frac{1}{\sqrt{2}}|00\rangle + |11\rangle$. This entangled state is created using the following circuit:

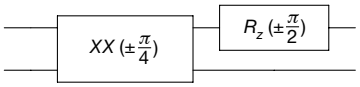

(3)

The sign of the XX gate depends on the pulse shape solution used for the particular gate, and is stored in a table in the control software, which then determines the appropriate Z rotation to create the Bell state. We use additional rotations to create the other Bell states from this circuit. We measure in the Bell basis by applying a simple CNOT gate followed by a Hadamard gate, and subsequent measurement of the two qubits.

Implementing and optimizing scrambling operators. The scrambling unitary used for the probabilistic teleportation scheme can be represented in the computational basis by the following matrix:

$$\hat{U}_s = \frac{1}{2}\begin{pmatrix} -1 & 0 & 0 & -1 & 0 & -1 & -1 & 0 \\ 0 & 1 & -1 & 0 & -1 & 0 & 0 & 1 \\ 0 & -1 & 1 & 0 & -1 & 0 & 0 & 1 \\ 1 & 0 & 0 & 1 & 0 & -1 & -1 & 0 \\ 0 & -1 & -1 & 0 & 1 & 0 & 0 & 1 \\ 1 & 0 & 0 & -1 & 0 & 1 & -1 & 0 \\ 1 & 0 & 0 & -1 & 0 & -1 & 1 & 0 \\ 0 & -1 & -1 & 0 & 1 & 0 & 0 & -1 \end{pmatrix} \quad (4)$$

Since this unitary is real, $\hat{U}_s^* = \hat{U}_s$, simplifying the experimental sequence since $\hat{U}_d = \hat{U}_s^* = \hat{U}_s$. The unitary fulfills the following set of equations which verify its scrambling property by showing that it delocalizes all single-qubit operators into three-qubit operators:

$$\begin{aligned} U^\dagger(X\otimes I\otimes I)U &= X\otimes Z\otimes Z \\ U^\dagger(I\otimes X\otimes I)U &= Z\otimes X\otimes Z \\ U^\dagger(I\otimes I\otimes X)U &= Z\otimes Z\otimes X \\ U^\dagger(Y\otimes I\otimes I)U &= Y\otimes X\otimes X \\ U^\dagger(I\otimes Y\otimes I)U &= X\otimes Y\otimes X \\ U^\dagger(I\otimes I\otimes Y)U &= X\otimes X\otimes Y \\ U^\dagger(Z\otimes I\otimes I)U &= Z\otimes Y\otimes Y \\ U^\dagger(I\otimes Z\otimes I)U &= Y\otimes Z\otimes Y \\ U^\dagger(I\otimes I\otimes Z)U &= Y\otimes Y\otimes Z \end{aligned} \quad (5)$$

where X, Y, Z and I are the three Pauli operators and the identity operator. This delocalization of local operators under time-evolution is a key signature of scrambling, and one can in fact relate the weight of these time-evolved local operators to the decay of (averaged) OTOCs analytically. The unitary $\hat{U}_s$ is implemented experimentally using six two-qubit entangling gates (see Extended Data Fig. 2).

In the experimental implementation, we take advantage of the following identity to reduce the number of two-qubit gates needed:

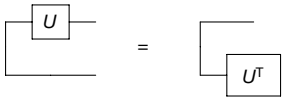

(6)

where the vertical line indicates that the qubits are in an EPR state.

In this way, we can combine the first two XX gates on ions 2 and 3 in $\hat{U}_s$ (and similarly on ions 4 and 5 in $\hat{U}_d$) into two single-qubit X-rotations, as shown in Extended Data Fig. 3.

In Fig. 2 we vary the amount of scrambling in U parametrized by α. This is achieved by changing the angles of the Z-rotations depicted in Extended Data Fig. 5 according to $\theta = \pm\frac{\alpha\pi}{2}$. When $\alpha = 0$, the XX-gates combine to create the identity matrix, and when $\alpha = 1$, the unitary corresponds to the maximally scrambling case shown in Extended Data Fig. 2. Additional Z-rotations are applied around the XX-gates to ensure that $\hat{U}_d = \hat{U}_s^*$. In Fig. 3, we measure the delocalization of information throughout the seven-qubit system in the presence of a maximally scrambling unitary $\hat{U}_s(\alpha = 1)$. The Bell measurements used are depicted in Extended Data Fig. 4 with the same colour scheme.

For the data in Fig. 4, we compose the scrambling unitary depicted in Extended Data Fig. 6. This unitary has the following matrix representation in the computational basis:

$$U_{CZ} = \frac{1}{2\sqrt{2}}\begin{pmatrix} 1 & 1 & 1 & -1 & 1 & -1 & -1 & -1 \\ 1 & -1 & 1 & 1 & 1 & 1 & -1 & 1 \\ 1 & 1 & -1 & 1 & 1 & -1 & 1 & 1 \\ -1 & 1 & 1 & 1 & -1 & 1 & -1 & 1 \\ 1 & 1 & 1 & -1 & -1 & 1 & 1 & 1 \\ -1 & 1 & -1 & -1 & 1 & 1 & -1 & 1 \\ -1 & -1 & 1 & -1 & 1 & -1 & 1 & 1 \\ -1 & 1 & 1 & 1 & 1 & 1 & 1 & -1 \end{pmatrix} \quad (7)$$

We can confirm that this is indeed a maximally scrambling unitary via a set of equations analogous to equation (5). The optimized circuit used to implement this unitary experimentally is shown in Extended Data Fig. 7. We use a similar circuit to effect the classical scrambling unitary, $\hat{U}_c$, by implementing only the first three controlled-Z gates.

Lastly, the Grover search operator labelled G in Fig. 4 is realized using the following circuit:

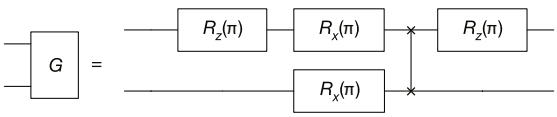

(8)

The SWAP gate (the line connecting two Xs) is implemented classically by reassigning qubit labels.

Numerical simulations. Theory curves were obtained through numerical simulation of the circuits in Methods section 'Implementing and optimizing scrambling operators' using a simple one-parameter coherent error model. To simulate coherent errors, a random single-qubit (or two-qubit) unitary close to the identity was applied following each single-qubit (or two-qubit) gate. Single-qubit rotations about the z-axis were performed classically with negligible experimental error and were therefore omitted from this procedure. Random single-qubit (or two-qubit) unitary errors were taken as the exponential of a linear combination of the three single-qubit (or 15 two-qubit) traceless Hermitian matrices, with coefficients sampled from a normal distribution with mean 0 and standard deviation $\epsilon/\sqrt{3}$ (or $\epsilon/\sqrt{15}$). The resulting observables $\langle P_\psi\rangle$ and $\langle F_\psi\rangle$ were averaged over $N = 10$ realizations of random error, and the same random errors were used for simulation at each experimental parameter. The error strengths $\epsilon = 0.232$ for the mismatch scan and $\epsilon = 0.174$ for the scrambling scan were chosen to minimize the sum of squared errors in $\langle P_\psi\rangle$ and $\langle F_\psi\rangle$. Deviations between simulations and data are probably caused by systematic errors, such as experimental drift and imperfect calibration. Furthermore, we expect the teleportation fidelities for the mismatch experiment in Fig. 2 to oscillate slightly around 50%. Instead, these data points are all just above 50%. This is probably caused by unwanted residual entanglement from the noise-inducing identity operators described in the main text.

Brief overview of quantum teleportation. Quantum teleportation is a process in which the quantum state of a particle (often, a qubit) is instantaneously

transferred to another identical particle[37]. Say Alice wants to teleport the state $|\psi\rangle$ of her qubit to Bob. To begin, Alice and Bob must share a maximally entangled state, for instance an EPR pair $(|00\rangle + |11\rangle)/\sqrt{2}$, where Alice possesses the first qubit of the EPR pair and Bob the second. This is a bizarre state, possible in quantum mechanics, in which each qubit individually has a completely undetermined quantum state, yet upon measurement the two qubits are guaranteed to be in identical states. To implement teleportation, Alice performs a certain EPR measurement on the two qubits in her possession, which succeeds with some finite probability. If successful, Bob's half of the EPR pair will be instantaneously transformed into the quantum state $|\psi\rangle$, and the state $|\psi\rangle$ will be erased from Alice's possession. Crucially, the finite success probability of Alice's measurement forbids Bob from knowing whether teleportation was successful until Alice communicates her result to him, preventing any faster-than-light transfer of information.

In our protocol Bob, not Alice, is the one to perform the measurement, and thus the instantaneity of the teleportation is not the focus. Rather, the teleportation serves as a component of our protocol to decode Alice's state after its scrambling by the unitary $\hat{U}$. If information of the state $|\psi\rangle$ is fully delocalized, that is, scrambled, by the unitary, teleportation can occur via measurement of any of the qubits acted on by the unitary—even those which initially contained no information about the state. The success of teleportation therefore serves as a diagnostic of scrambling.

Brief overview of Grover's algorithm. Grover's algorithm is a quantum search algorithm, and one of the premier instances of a task that a quantum algorithm can perform provably faster than any classical algorithm[31]. In it one associates a set of quantum states with items of a database, and attempts to search for a given item of the database. To perform the algorithm, one begins by initializing a quantum state that is an equal superposition of all possible database states. The search process involves repeated applications of an 'oracle' operator, which flips the phase of the searched-for state, alternating with an 'amplification' operator, which reflects the superposition about its mean amplitude. After each pair of operations the amplitude of the searched-for state is increased, and a measurement of the state of the system will return the searched-for state with increasing probability. An order unity success rate can be achieved in $O(\sqrt{N})$ steps, a quadratic speedup over the $O(N)$ steps required in a classical search of an unsorted database.

In our protocol we search for an EPR pair on qubits (3, 4) in a two-qubit database, that is, $N = 2^2 = 4$. In this particular case of $N = 4$, Grover's algorithm in fact succeeds with probability 1 after just one application of the oracle operator, which involves the unitaries $\hat{U}^\top$ and $\hat{U}^*$ and the Grover search operator[5] G.

Data availability

All relevant data are available from the corresponding author upon request.

34. Mølmer, K. & Sørensen, A. Multiparticle entanglement of hot trapped ions. *Phys. Rev. Lett.* **82**, 1835 (1999).
35. Zhu, S.-L., Monroe, C. & Duan, L.-M. Arbitrary-speed quantum gates within large ion crystals through minimum control of laser beams. *Europhys. Lett.* **73**, 485–491 (2006).
36. Choi, T. et al. Optimal quantum control of multimode couplings between trapped ion qubits for scalable entanglement. *Phys. Rev. Lett.* **112**, 190502 (2014).
37. Bennett, C. H. et al. Teleporting an unknown quantum state via dual classical and Einstein-Podolsky-Rosen channels. *Phys. Rev. Lett.* **70**, 1895–1899 (1993).

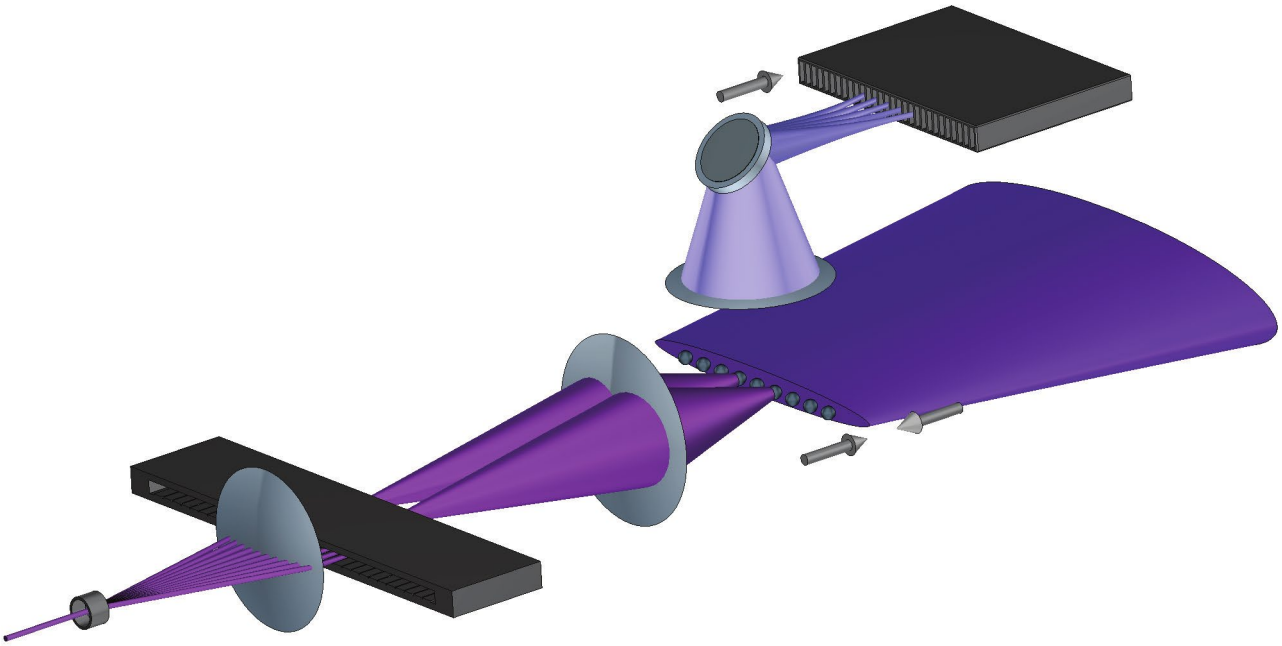

Extended Data Fig. 1 | Experimental apparatus. Horizontal, dark-purple counter-propagating laser beams are illustrated with a large global beam illuminating one side of the chain and two of the seven individually modulated, tightly focused beams on the other side. The middle seven of the nine $^{171}Yb^{+}$ ions are imaged, which allows us to address each qubit independently. Individual addressing is accomplished by imagining each ion onto an individual photomultiplier tube. The light purple, vertical light cones represent light collection from the ions onto the photomultiplier tubes.

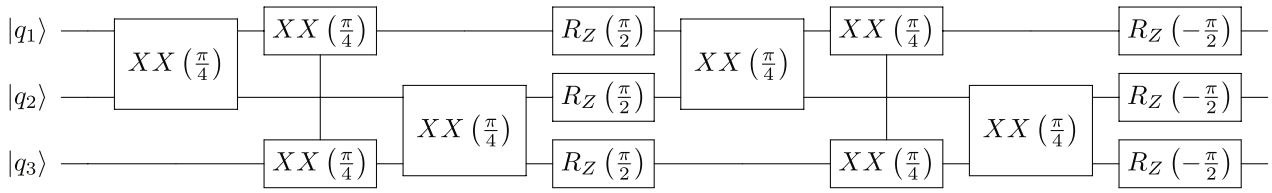

Extended Data Fig. 2 | Circuit representation of the scrambling unitary used for the probabilistic teleportation scheme. See equation (4). The scheme consists of six two-qubit entangling XX-gates and individual Z-rotations.

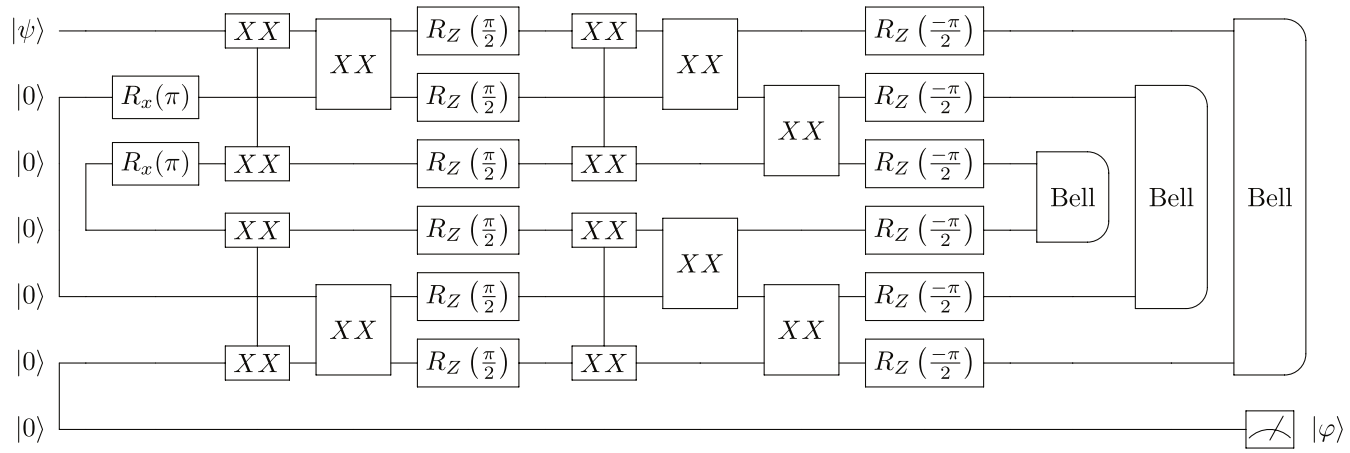

Extended Data Fig. 3 | Experimental sequence used for the probabilistic teleportation scheme. Any one of the three Bell measurements can be used. The scrambling unitary has been simplified using the identity given in equation (6).

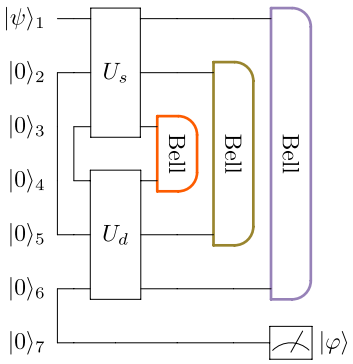

Extended Data Fig. 4 | Circuit depicting the Bell measurement pairs used in Fig. 3a and b.

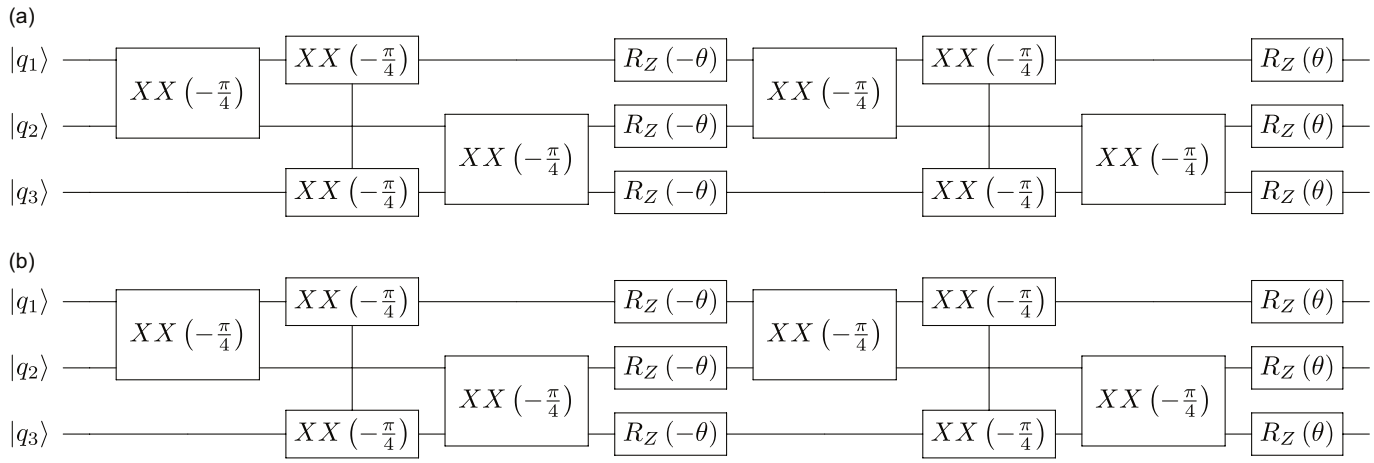

Extended Data Fig. 5 | Circuit depicting experiment from Fig. 2. **a**, Circuit for the unitary used in Fig. 2. **b**, The same unitary with varying degrees of scrambling for the data in Fig. 2. The angles of the Z-rotations are changed according to $\theta = \pm\frac{\alpha\pi}{2}$ to continuously scan between not scrambling ($\alpha = 0$) and maximally scrambling ($\alpha = 1$).

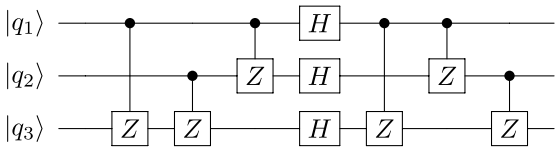

Extended Data Fig. 6 | Circuit representation of the scrambling unitary from equation (7), used for the data in Fig. 4. The breakdown into native gates for the experimental implementation is shown in Extended Data Fig. 7. A reduced circuit, made up of only the first three controlled-Z gates, is used to create the classical scrambling unitary $\hat{U}_c$.

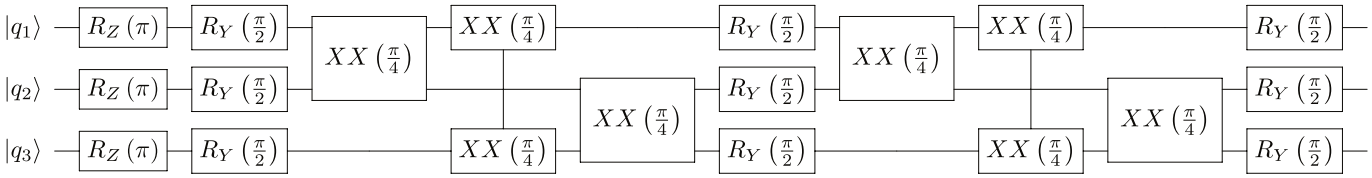

Extended Data Fig. 7 | The scrambling unitary from equation (7) compiled into native gates. This circuit was used for the measurements in Fig. 4.